Origin of exchange bias in $[Co/Pt]_{ML}$/Fe multilayers with orthogonal magnetic anisotropies

Sadhana Singh,[1,2] Avinash G. Khanderao,[1,3] Mukul Gupta,[1] Ilya Sergeev,[4] H. C. Wille,[4] Kai Schlage,[4] Marcus Herlitschke,[4] and Dileep Kumar[1,*]

[1]*UGC-DAE Consortium for Scientific Research, Khandwa Road, Indore 452017, India*

[2]*Nanomagnetism and Microscopy Laboratory, Department of Physics, Indian Institute of Technology Hyderabad, Kandi, Sangareddy, Telangana 502285, India*

[3]*Department of Physics, Jagadamba Mahavidyalaya, Achalpur City, Maharashtra 444806, India*

[4]*Deutsches Elektronen-Synchrotron DESY, Notkestraße 85, 22607 Hamburg, Germany*

(Received 20 July 2022; revised 18 May 2023; accepted 28 July 2023; published 14 August 2023)

Magnetization reversal of a soft ferromagnetic Fe layer coupled to a $[Co/Pt]_{ML}$ multilayer (ML) with perpendicular magnetic anisotropy (PMA) has been studied *in situ* with an aim to understand the origin of exchange bias (EB) in orthogonal magnetic anisotropic systems. The interface remanent state of the ML is modified by magnetic field annealing, and its effect on the soft Fe layer is monitored using the *in situ* magneto-optical Kerr effect (MOKE). A considerable shift in the Fe layer hysteresis loop from the center and an unusual increase in the coercivity, similar to EB phenomena, is attributed to the exchange coupling at the $[Co/Pt]_{ML}$ and Fe interface. The effect of the coupling on spin orientation at the interface is further explored precisely by performing an isotope selective grazing incident nuclear resonance scattering (GINRS) technique. Here, the interface selectivity is achieved by introducing a 15 Å-thick Fe^{57} marker between the $[Co/Pt]_{ML}$ and Fe layers. The interface signal from Fe^{57} is further enhanced by performing measurements under x-ray standing-wave conditions. The combined MOKE and GINRS analysis revealed a unidirectional pinning of the Fe layer due to the net in-plane magnetic spin at the interface caused by magnetic field annealing. Unidirectional exchange coupling or pinning at the interface, which may be due to the formation of asymmetrical closure domains, is found to be responsible for the origin of EB with an unusual increase in coercivity.

DOI: 10.1103/PhysRevB.108.075414

I. INTRODUCTION

Exchange bias (EB) refers to the shift of the hysteresis loop along the magnetic field axis when the antiferromagnetic (AFM)/ ferromagnetic (FM) system is field-cooled (FC) below the Néel temperature (T_N) of the AFM layer [1–3]. This occurs due to unidirectional anisotropy induced in the FM layer due to exchange interaction at the interface [1–3]. Hard/soft FM bilayers exhibit a similar phenomenon due to the pinning of soft-layer magnetization by the hard layer [4–8]. However, this pinning is a collective effect of direct exchange interaction at the interface and dipolar interaction due to stray fields [4–6,8]. Depending on the direction of field cooling [2,3,9–12] of the AFM layer or saturation of the hard layer [4–8,13–15], in-plane [2,4–7] or perpendicular EB [2,9–11,13–15] can be induced in magnetic thin films. In most studies, the AFM and hard FM layer have magnetic anisotropy coplanar to the magnetic anisotropy of the soft FM layer [2,4–7]. However, there are a few studies that report the occurrence of EB in the system with orthogonal magnetic anisotropy (OMA), such as $[Co/Pt]_n$/NiFe [16–19], GaMnAsP/GaMnAs [20], $Co_{0.66}Cr_{0.22}Pt_{0.12}$/Ni [21], Py/YIGBiLuAl [22], $[Co(0.2)/Pd(1)]_5$/CoFeB [12], [Pd/Co]/Cu/Co/Cu/[Co/Pd] [23], etc. Here, the soft FM layers have in-plane magnetic anisotropy (IMA), whereas the hard layers have perpendicular magnetic anisotropy (PMA). There is ongoing research to explore new materials and investigate the various factors that contribute to biasing, with an aim toward achieving tunable and robust EB at room temperature. The continuous efforts in this field are driven by the desire to enhance the understanding of EB phenomena and unlock their potential for practical applications.

The appearance of EB in such systems was first reported by Sort *et al.* [16] in 2004. According to them, in-plane EB can be induced in a $[Co/Pt]_n$/NiFe system having OMA by applying a very high in-plane magnetic field. Later, similar results were reported in various other systems, as listed above [12,17–19,21–23]. It was concluded that the orientation of spins at the interface between the soft IMA layer and the hard PMA layer plays the main role in the appearance of EB. The application of a large magnetic field changes the interface domain structure, which in turn affects the orientation of spins at the interface, thereby leading to the pinning of the soft layer and EB. As per Bollero *et al.* [18], the asymmetry and stability of vortices between the upward and downward domains during magnetization reversal might play an important role in inducing EB. It is reported that EB can be further tuned by modifying the strength of the PMA layer through the buffer layer [18], patterning long parallel strips instead of the continuous film [24] or applying an external perpendicular

*Corresponding author: dkumar@csr.res.in; dileep.esrf@gmail.com

magnetic field [12]. Recently, a similar EB was reported in the FM semiconductor GaMnAsP/GaMnAs bilayer with OMA [20] when FC in the strong in-plane magnetic field.

Although most of the above studies point out the importance of the orientation of the interface spins for the origin of EB in OMA systems, a proper depth-selective study to probe the interface magnetism is missing. So far, only indirect magnetic characterization techniques such as the magneto-optical Kerr effect (MOKE), a vibrating sample magnetometer (VSM) [16,18,19,21], the Hall effect [17,20], and magnetic force microscopy (MFM) [16–18], as well as micromagnetic theoretical simulations [17,18,22], have been utilized to explain the origin of EB in these systems. However, these techniques provide average information on the magnetic behavior of the multilayer, and they are not depth-selective. Thus, they do not provide direct information on the orientation of moments at the interface. Since the interface plays a significant role, a detailed depth-resolved study is required to determine the net magnetization direction at the IMA and PMA layer interface to understand the origin of EB. Depth-sensitive techniques such as conversion electron Mössbauer spectroscopy (CEMS), polarized neutron reflectivity (PNR) [21], and x-ray magnetic circular dichroism (XMCD) are more informative and powerful methods for interface-mediated studies. However, each has its limitations, such as limited penetration depth, low resonance counts, large sample size, long measurement time, etc. [25]. Thus, probing a particular interface in a multilayer system cannot be helpful. In such cases, synchrotron-based grazing incident nuclear resonance scattering (GINRS) with isotope sensitivity and high scattering yield can be used as an effective tool for depth-resolved measurement by placing a marker layer of the isotope at the designated depth.

Considering the above points, we have studied the origin of EB in $[Co/Pt]_{ML}$/Fe multilayers, where $[Co/Pt]_{ML}$ is prepared with strong PMA and Fe with in-plane anisotropy. *In situ* MOKE is performed after annealing a multilayer at different temperatures in the magnetic field. Magnetization reversal of the Fe layer coupled to $[Co/Pt]_{ML}$ is studied using *in situ* MOKE after annealing samples to varying temperatures in the magnetic field. The results are also compared with the samples annealed without the magnetic field. Furthermore, GINRS measurement, analogous to Mössbauer spectroscopy, was performed to obtain the interface-resolved magnetism and relative orientation of the Fe magnetic moment (μ_{Fe}) at the interface. For this purpose, a thin probe layer of isotopic Fe^{57} was deposited at the interface between the $[Co/Pt]_{ML}$ and Fe layer [26]. In addition, the x-ray standing-wave (XSW) technique under planar waveguide conditions was utilized to enhance resonantly scattered counts from the Fe^{57} isotope marker layer. The present study provides direct evidence of the spin structure at the interface and its role in inducing EB in the multilayer with two orthogonal anisotropies.

II. EXPERIMENT

Pt (250 Å)/[Co (6 Å)/Pt (30 Å)]$_{10}$/Co (5 Å)/Fe^{57} (20 Å)/Fe(70 Å)/Pt (30 Å) multilayer [Fig. 1(a)] with an Fe^{57} marker layer at the $[Co/Pt]_{ML}$-Fe interface was deposited at room temperature (RT) using a magnetron sputtering technique

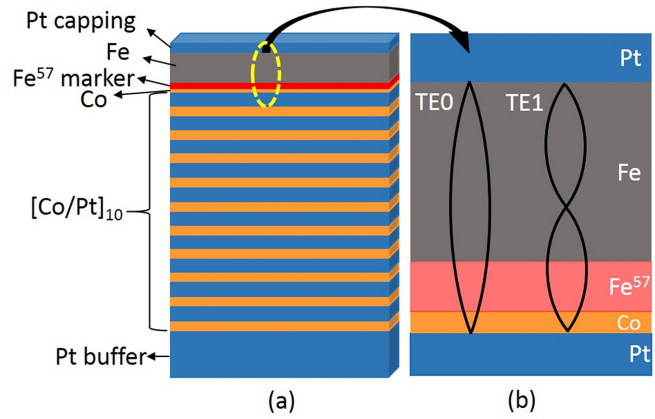

FIG. 1. Schematic diagrams showing (a) $[Co/Pt]_{ML}$/Fe multilayer structure and (b) enlarged view of XSW formation through planar waveguide structure between the top two high-density Pt layers.

on Si (111) substrate at a base pressure of 5.7×10^{-7} Torr. The multilayer will be denoted as $[Co/Pt]_{ML}$/Fe for ease of reading. It may be noted that a thin Co layer of about 5 Å thickness was deposited on top of $[Co/Pt]_{ML}$ (before Fe^{57} deposition) to enhance PMA and avoid interdiffusion between Pt and Fe^{57} layers directly [9]. High-density layers (Pt) of thicknesses 250 and 30 Å are deposited, respectively, as a buffer and capping to enhance PMA [13,27], avoid surface oxidation, and generate XSW [25,28–30]. In the present case, the top two Pt layers act as walls of the planar waveguide, whereas the Co/Fe^{57}/Fe structure acts as a guiding layer [25,28–30]. A schematic of the formation of XSW in the guiding layer is shown in Fig. 1. Two pieces of the same multilayer sample were annealed at various temperatures in ultrahigh-vacuum (UHV) conditions. One of the samples was annealed in the presence of a 1.5 kOe in-plane magnetic field (designated as "H-annealing"), whereas the other sample was annealed in the absence of a magnetic field in identical vacuum conditions. MOKE in polar geometry (P-MOKE) was performed to confirm PMA in the $[Co/Pt]_{ML}$ multilayer, whereas magnetization reversal of the Fe layer is studied by collecting a hysteresis loop after different annealing stages using longitudinal MOKE (L-MOKE) measurements. It may be noted that hysteresis loops were measured at RT in a ±250 Oe magnetic field, which is much less than the magnetic field required to disturb the magnetization reversal of $[Co/Pt]_{ML}$ multilayer due to PMA. See the supplemental material for details on selecting the appropriate magnetic field for the hysteresis loop measurement [31] (see also Refs. [32,33] therein). The hysteresis loops presented in this work correspond to the soft magnetic structure on a $[Co/Pt]_{ML}$ multilayer unless specified.

GINRS experiments were carried out under XSW using an x-ray synchrotron radiation source at the P01, Dynamics Beamline at PETRA III, DESY, Hamburg, Germany [34]. Interface selectivity was achieved due to crossing XSW antinodes with the interface at an appropriate x-ray incident angle [30,35,36]. The correct angle of the incident ($q = 0.066$ Å^{-1}) to perform GINRS measurements is extracted based on electronic and nuclear reflectivity measurements.

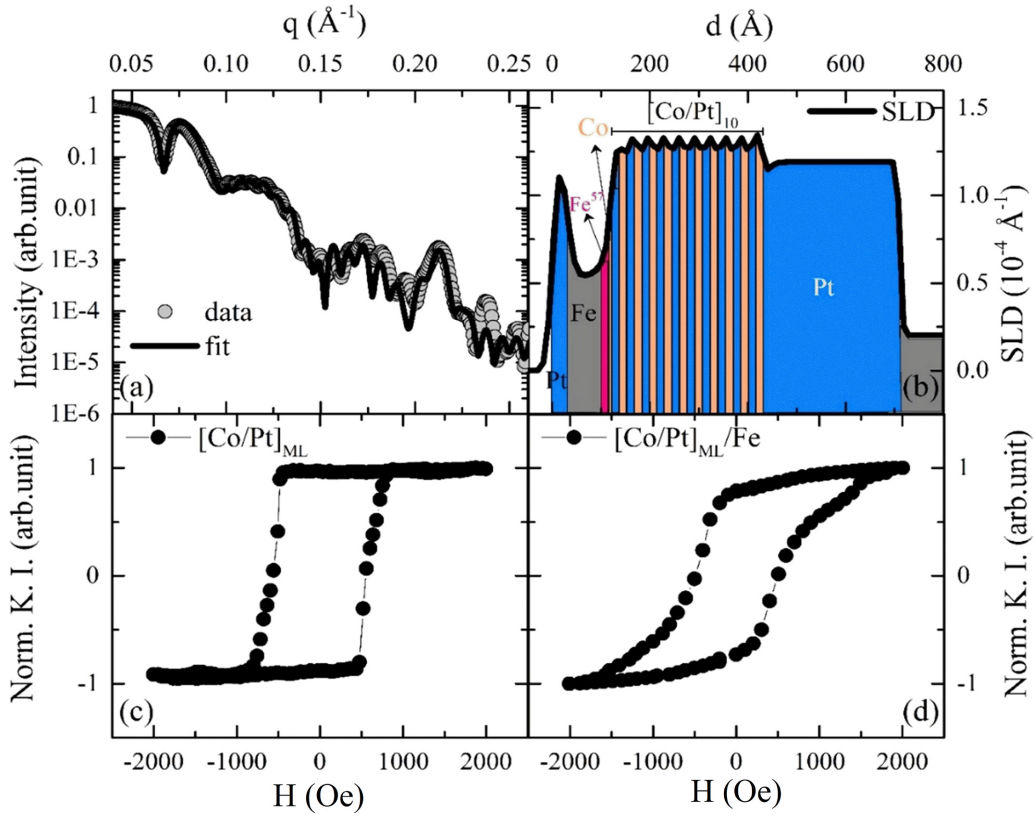

FIG. 2. (a) Fitted XRR pattern and (b) extracted scattering length density (SLD) profile of as-deposited $[Co/Pt]_{ML}$/Fe multilayer. P-MOKE hysteresis loop of (c) $[Co/Pt]_{ML}$ and (d) $[Co/Pt]_{ML}$/Fe.

GINRS experiments are conducted in a time mode with a beam having 40 bunch with a bunch separation of 192 ns. The x-ray energy was tuned to 14.41 keV, the nuclear transition energy corresponding to the Fe^{57} Mössbauer isotope with a natural lifetime of 141 ns.

III. RESULT AND DISCUSSION

Figure 2(a) shows the x-ray reflectivity (XRR) pattern (circles) of the as-deposited $[Co/Pt]_{ML}$/Fe multilayer fitted (solid line) using Parratt's formalism [37]. The corresponding extracted scattering length density (SLD) profile from XRR fitting is shown in Fig. 2(b). Small oscillations in the XRR pattern signify the total thickness of the multilayer, whereas Bragg's peak at $\sim q$ (momentum transfer vector perpendicular to the surface)$= 0.21$ Å^{-1} corresponds to the bilayer thickness of $[Co/Pt]_{ML}$. After fitting, the thickness of Co and Pt layers in $[Co/Pt]_{ML}$ is found to be 4.6 Å (±0.2 Å) and 26.5 Å (±0.5 Å), respectively, whereas Fe layer thickness is about ∼ 85 Å (including Fe^{57} thickness). It may be noted that Fe^{57} and Fe^{Nat} are chemically the same (same electron density in both isotopes); therefore, the XRR technique gives combined information on the Fe^{57} and Fe^{Nat} layers. The sharp dip around $q = 0.066$ Å^{-1}, below the critical angle of Pt, indicates the resonance coupling of incident x-rays resulting from the waveguide between two high-density Pt layers in top **Pt**/Co/Fe^{57}/Fe/**Pt** layers [25,28–30]. The final sample structure obtained after XRR fitting is Pt (240 Å)/$[Co\ (4.6\ Å)/Pt\ (26.5\ Å)]_{10}$/Co (4 Å)/$Fe^{57}$ (15 Å)/Fe(70 Å)/Pt (30 Å).

Figures 2(c) and 2(d) show the P-MOKE hysteresis loop of $[Co/Pt]_{ML}$ and $[Co/Pt]_{ML}$/Fe multilayers separately. It is observed that $[Co/Pt]_{ML}$ multilayer exhibits an almost square hysteresis loop with very high remanence (Mr = 0.94) and low coercivity ($H_C \sim 560$ Oe). It clearly shows that the $[Co/Pt]_{ML}$ multilayer exhibits strong PMA. The origin of PMA in this multilayer is known to originate from the spin-orbit coupling between Co and Pt atoms [38,39]. The hysteresis loop of $[Co/Pt]_{ML}$/Fe is expected to be a combination of two loops. A square loop corresponds to $[Co/Pt]_{ML}$ with a magnetic easy axis along the direction of the applied field, and the slanted loop corresponds to the Fe layer with an easy axis along the in-plane direction. Thus, the magnetic reversal of $[Co/Pt]_{ML}$ occurs in relatively less field than the Fe layer. In the present case, the hysteresis loop of $[Co/Pt]_{ML}$/Fe needs a larger field (>2000 Oe) to achieve saturated magnetization reversal in this geometry. Because of this fact, with the magnetic field strength of ±2000 Oe, both the Fe layer and $[Co/Pt]_{ML}$ participate in the magnetic reversal process resulting in a combined loop in P-MOKE. Furthermore, the hysteresis loop of the $[Co/Pt]_{ML}$/Fe multilayer was measured in ±250 Oe at RT in L-MOKE geometry. In L-MOKE geometry, the magnetic field ±250 Oe is sufficient for the magnetization reversible of the Fe layer but is much less than the field required to switch $[Co/Pt]_{ML}$ structure.

As shown in Fig. 3, the loops exhibit an almost single-step square hysteresis loop along two in-plane azimuthal directions $\theta = 0°$ and 90°. Both loops are almost similar in shape, confirming isotropic Fe magnetism in the film plane. The loops

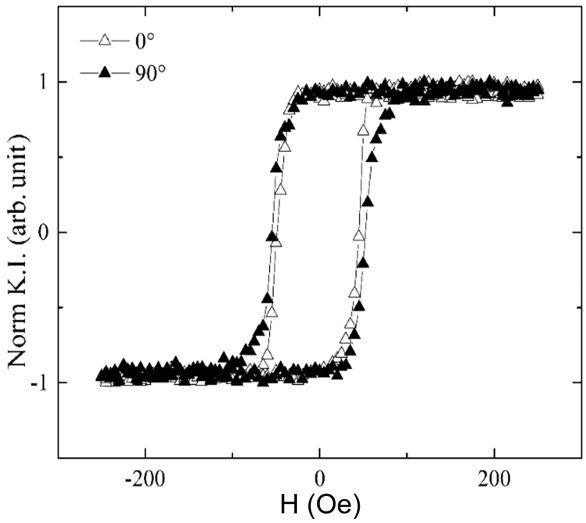

FIG. 3. L-MOKE hysteresis loop of $[Co/Pt]_{ML}/Fe$ in ±250 Oe magnetic field along azimuthal angles $\theta = 0°$ and 90° ($\theta = 0°$ is any arbitrary azimuthal direction).

are also centered in the magnetic field axis (x-axis), indicating the absence of preferential pinning in the film. Hence, no EB is present in the as-deposited stage.

Prior to the EB study, the thermal stability of the multilayer was investigated by collecting hysteresis loops of the multilayer layer in a magnetic field ±250 Oe (L-MOKE geometry) and XRR patterns after annealing samples at different temperatures up to 673 K. All hysteresis loops are presented in Fig. 4. It is observed that with increasing annealing temperature, the H_C of the multilayer first decreases up to 473 K. However, an unusual increase in H_C was observed after annealing at 523 K. All the hysteresis loops remain centered

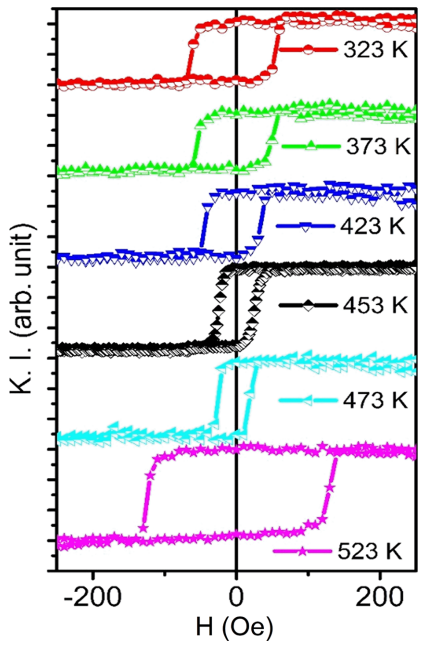

FIG. 4. L-MOKE hysteresis loop of $[Co/Pt]_{ML}/Fe$ multilayer after annealing at different temperatures under UHV conditions.

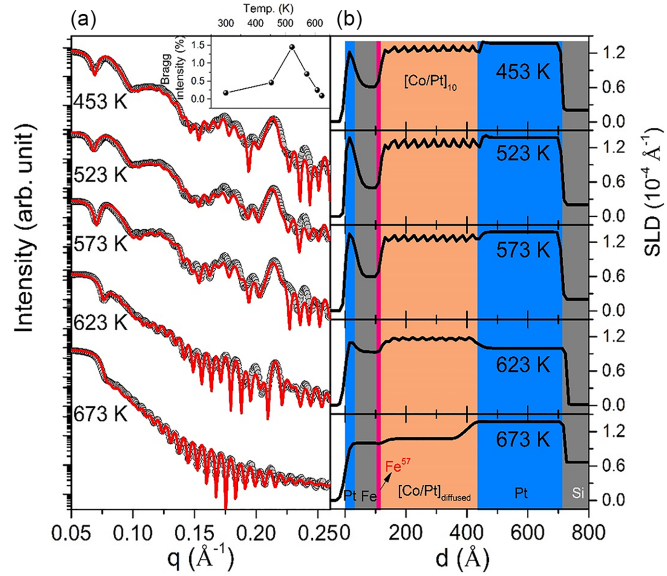

FIG. 5. (a) Fitted XRR pattern and (b) SLD profile of $[Co/Pt]_{ML}/Fe$ multilayer after annealing it at different temperatures under UHV conditions. The inset gives the normalized Bragg peak intensity variation after annealing the sample up to 673 K.

along the field axis, hence no preferential coupling between hard $[Co/Pt]_{ML}$ and soft Fe layers is induced after annealing. Initial decreases in H_C with increasing annealing temperatures can be understood in terms of the removal of stress or defects which might have been generated during film growth. The unusual increase in H_C after annealing at 523 K may be due to (i) increased interface domain-wall pinning at the interfaces due to interdiffusion, or (ii) an increase in isotropic coupling between hard $[Co/Pt]_{ML}$ and soft Fe layers.

The XRR measurements of the multilayer were carried out after annealing at different temperatures ranging from 453 to 673 K [see Fig. 5(a)] to correlate the structural properties (layer thickness, interface roughness, and interface mixing) with the evolution of magnetic properties after annealing. All XRR patterns are shown in Fig. 5(a), where solid lines represent the best fit to the data using Parratt's formalism [37]. The corresponding SLD profiles, extracted after fitting, are shown in Fig. 5(b). The normalized Bragg peak intensity increases with annealing up to 523 K [inset Fig. 5(a)]. With further annealing, it decreases at 623 K and finally disappears after annealing at 673 K. After annealing at this temperature, the XRR pattern consists of only the total thickness oscillations (Kiessig oscillations). As Bragg peak intensity is directly related to the interface roughness of $[Co/Pt]_{ML}$ [40,41], the initial increase in Bragg peak intensity clearly suggests that the Co/Pt interfaces became sharp due to interface demixing up to 523 K. Sharpening of the $[Co/Pt]_{ML}$ interfaces can also be seen in SLD profiles corresponding to the temperatures 453 and 523 K. The decrease in Bragg intensity beyond 523 K is mainly due to diffusion at the interface across the layers of the multilayer. Complete intermixing of Co and Pt layers at 623 K results in the disappearance of the Bragg peak. Similar observations have also been reported in the literature where such multilayers are stable up to moderate temperature.

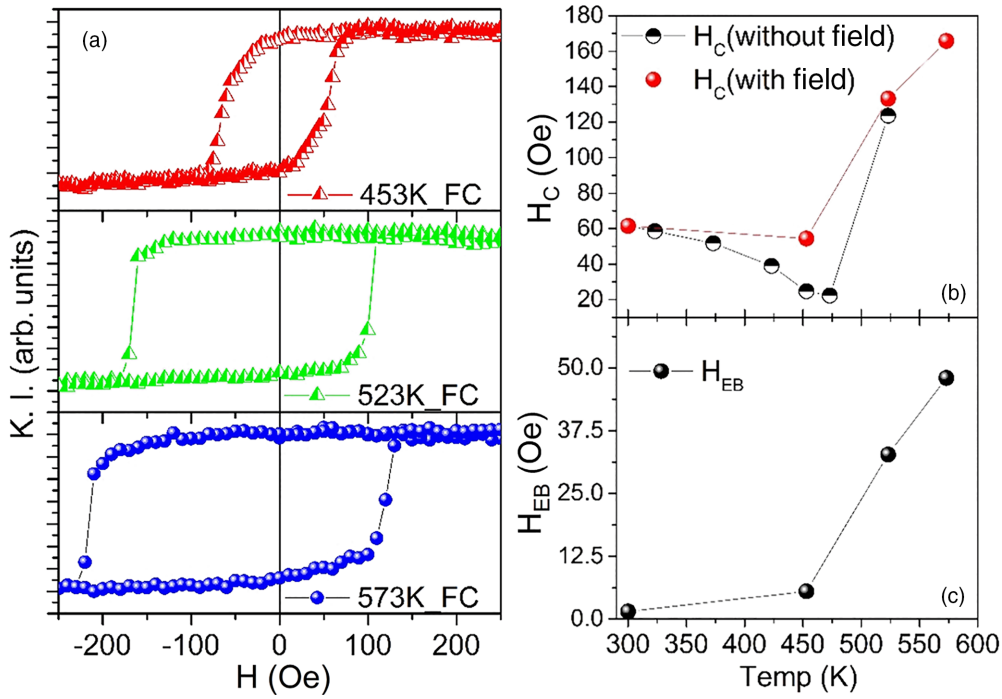

FIG. 6. (a) Hysteresis loop of $[Co/Pt]_{ML}$/Fe multilayer after annealing in the presence of ∼ 1500 Oe magnetic field. Variation of (b) H_C (with and without field annealing) and (c) H_{EB} with increasing annealing temperature.

Interdiffusion occurs with a further increase in the temperature [39,42–45] and is responsible for decreased PMA in the Co/Pt multilayer systems. The effect of thermal annealing has also been studied separately on the same $[Co/Pt]_{ML}$ by performing P-MOKE. See the supplemental material for the decreasing strength of PMA with increasing temperature above 523 K [31].

Figure 6(a) shows hysteresis loops of the sample measured at RT after H-annealing at different temperatures in the presence of ∼ 1.5 kOe magnetic field. On H-annealing up to 453 K, the hysteresis loop remains centered at the magnetic field axis. However, for temperatures 523 K and above, hysteresis loops are shifted from their origin. This shift is higher with a further increase in temperature up to 573 K. This observation clearly suggests the appearance of the EB at these H-annealed states.

Figures 6(b) and 6(c) show the variation of H_C and H_{EB} with increasing temperature for qualitative understanding. H_{EB} variation with temperature in Fig. 6(c) gives the slow increase of EB up to 450 K. But with a further increase in temperature up to 573 K, it drastically increases in EB (H_{EB} = 6 to 50 Oe). In Fig. 6(b), H_C variation shows a drastic increase in the H_C beyond H-annealing at ∼ 450 K. Its value is almost double compared to the annealing in the absence of field. It is clear that the modified interface spin structure, due to the H-annealing, is the main factor that plays an important role in the origin of EB in this sample.

Figure 7 shows three hysteresis loops of $[Co/Pt]_{ML}$/Fe multilayer measured at RT after (i) annealing at 473 K in the absence of field, (ii) field annealing along 0°, and (iii) field annealing along 0° and measurements along the 180° direction. In the latter two cases, the loops show a positive and negative shift with almost the same strength. The opposite sign of EB in the last case confirms the exchange bias genuineness and negates its occurrence due to the minor loops.

To investigate the role of interface magnetism, depth-selective GINRS measurements are performed to probe magnetism (hyperfine field and spin orientation) at the interface for H-annealed samples. As GINRS is an isotope-sensitive technique, a thin Fe^{57} layer is used as a marker layer at the $[Co/Pt]_{ML}$ and Fe interface. Since the Fe^{57} layer is very thin, the XSW technique [25,28–30,46] is utilized to enhance the resonance counts from the marker layer at the

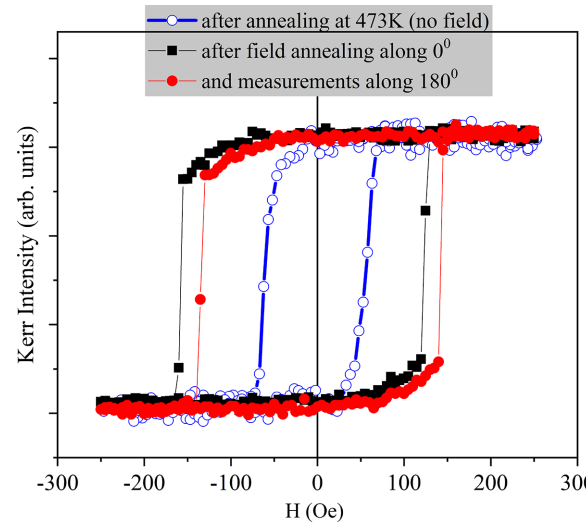

FIG. 7. Hysteresis loops measured at RT (a) after annealing at 473 K, (b) after field annealing along 0°, and (c) after field annealing along 0° and measurements along 180°.

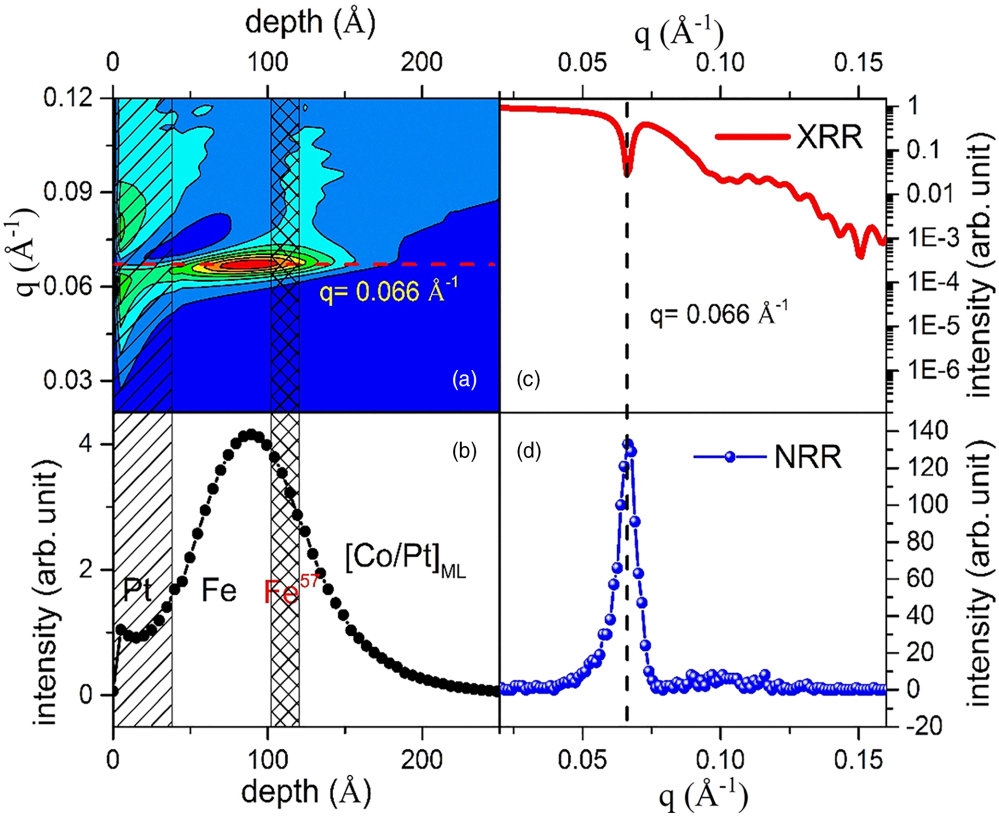

FIG. 8. (a) Contour plot of x-ray field intensity inside $[Co/Pt]_{ML}$/Fe multilayer as a function of depth and scattering vector q. (b) Electric field intensity (EFI) extracted for an angle of incidence of $q = 0.066\,\text{Å}^{-1}$. XSW antinode (TE0 mode) crosses the Fe^{57} marker layer at this angle. Experimental (c) nonresonant and (d) resonant reflectivity of the multilayer showing minima and maxima, respectively, at $q = 0.066\,\text{Å}^{-1}$.

interface. In the XSW technique, x-ray electric field intensity (EFI) is confined to different XSW modes (nodes and antinodes). By varying the angle of incidence, the position of the antinodes can be moved along the z-direction (depth) [30,35,36]. Enhanced nuclear resonance yield can be achieved by moving the antinode position across the marker layer at a particular incident angle. Based on the final sample structure, as obtained from the XRR measurements, x-ray EFI inside the guiding layer was calculated as a function of scattering vector q (incident angle θ) using Parratt's formalism [37] and shown in Fig. 8(a).

Clear confinement of the EFI (TE0 mode) was observed at around the angle of incidence $\theta = 0.259^\circ$ ($q = 0.066\,\text{Å}^{-1}$) and crosses the Fe^{57} layer at the interface. It suggests that GINRS measurement at $q = 0.066\,\text{Å}^{-1}$ will increase the nuclear resonance counts from the Fe^{57} layer. To further confirm it experimentally, nuclear resonance reflected intensity is collected as a function of q along with XRR and shown in Figs. 8(c) and 8(d). More than an order of magnitude higher resonant intensity has been observed at around $q = 0.066\,\text{Å}^{-1}$. In view of the above facts, all GINRS measurements (time spectra) were recorded at an incidence angle of $q = 0.066\,\text{Å}^{-1}$ for the H-annealed multilayer at various temperatures.

For the GINRS measurements, samples were placed in the path of the beam such that the direction of the magnetic field applied during annealing is normal to the scattering plane of the incident beam. Figure 9(a) shows a schematic representation of sample orientation with respect to the x-ray beam. Here, k_i and k_f denote the incident and reflected wave vectors, and θ represents the incident angle of the synchrotron beam. B is the angle of the hyperfine field (BHf) along the saturation field direction (γ) with respect to the plane normal. Figure 9(b) gives the temperature-dependent GINRS curves obtained at $q = 0.066\,\text{Å}^{-1}$. To get the Bhf and distribution of the hyperfine field, all curves are fitted using the simulation and least-squares fitting procedure of the REFTIM software [47,48] by taking the multilayer structure as obtained from XRR and NRR measurements. The best fit to the data is obtained by dividing the Fe^{57} layer into two layers ($Fe^{57}_{top} \sim 8$ Å and $Fe^{57}_{int} \sim 7$ Å) and considering three different hyperfine field (Bhf) components 32.9 ± 0.02, 32.6 ± 0.015, and 28.7 ± 0.09 T in both layers. Based on the fitting, the percentage of density concentration of all the Bhfs in Fe^{57} layers is presented in Table I. It may be noted that the percentage compositions of the Bhfs are hardly affected by the temperature. On the other hand, their alignments and relative contribution are different within the Fe^{57} layer (in Fe^{57}_{top} and Fe^{57}_{int} layers) due to the different magnetism caused by compositional differences and the interface proximity.

It is found that the interface layer has a higher contribution ($\sim 12\%$) of reduced hyperfine field (28.7 ± 0.79 T), which is hardly influenced by the annealing temperatures. It increases slightly (from 12% to 15%) in the interface part of the Fe^{57}

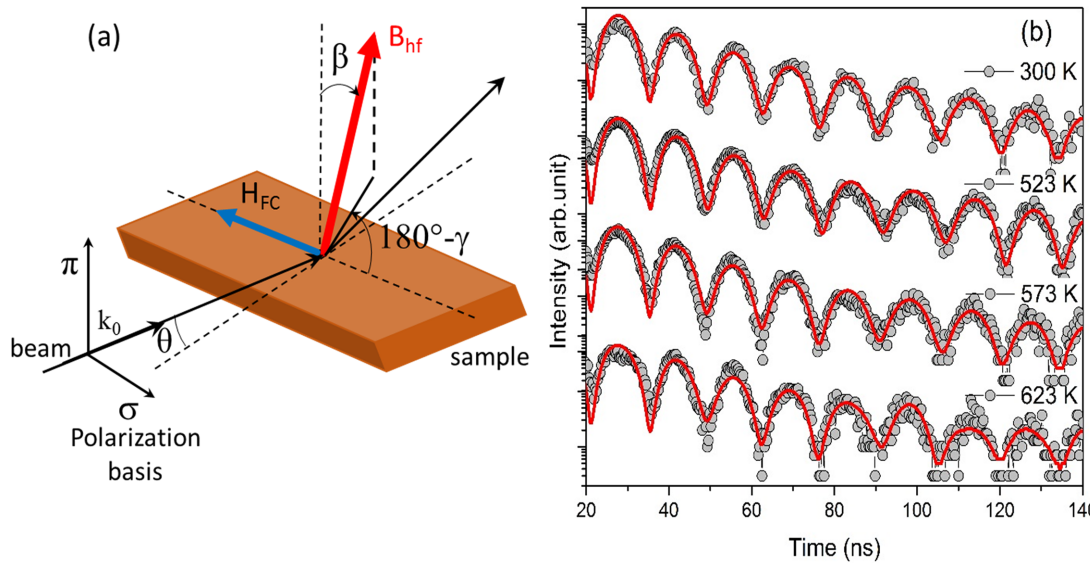

FIG. 9. (a) Schematic representation of the orientation of the sample with respect to the scattering plane and magnetic field applied during annealing. θ is the angle of incidence of the beam with respect to the sample surface. (b) GINRS time spectra of $[Co/Pt]_{ML}$/Fe multilayer after annealing at various temperatures and cooling to RT in an in-plane magnetic field (∼1500 Oe). Spectra are fitted using REFTIM software [47].

layer after annealing at 623 K. This may be due to interfacial mixing after annealing. The direction of Bhfs is defined in terms of two angles, namely angle β with respect to the surface normal, and the azimuthal angle γ with respect to the direction of polarization of x-rays. The azimuthal angle γ was kept around 0° during measurement. A small variation in the value γ (±2°) was considered in order to optimize the fitting. This variation in γ could be due to some misalignment of the sample with respect to the beam. After annealing, the systematically increasing value of β confirms spin alignment away from the film normal. At room temperature (300 K), spins of the Fe^{57} layer are oriented almost perpendicular to the film plane ($\beta = 0°-2°$). After field annealing at 623 K, the net magnetization rotates by approximately 34° (±1°) with respect to the plane normal (β) along the saturation field direction (γ). The rotation of moments in the in-plane direction may be attributed to pinning caused by magnetic field annealing.

TABLE I. Fitting parameter of GINRS spectra obtained using REFTIM software [47,48]. Errors in angle β are ±1°.

		Percentage Bhf		
Temp.	Bhf (T) (total%)	$^{57}Fe_{top}(d = 8$ Å)	$^{57}Fe_{int}(d = 7$ Å)	β (deg)
300 K	32.89 (64%)	34%	30%	2
	32.61 (22%)	12%	10%	0
	28.75 (14%)	2%	12%	0
523 K	32.85 (64%)	34%	30%	14
	32.75 (21%)	11%	10%	11
	28.25 (15%)	2%	13%	9
573 K	32.90 (63%)	34%	29%	16
	32.61(21%)	11%	10%	11
	28.29 (16%)	2%	14%	13
623 K	32.94 (62%)	33%	29%	34
	32.44 (21%)	11%	10%	34
	27.78 (17%)	2%	15%	34

As per Refs. [49–51], when a soft FM layer is deposited on a layer with strong PMA, the soft FM layer moments are aligned perpendicular for thicknesses below the exchange length. With increasing thickness, the moments gradually rotate in-plane. Furthermore, a gradual rotation of moments occurs within the layer even for a constant thickness of the soft FM layer [51]. In the present case, $[Co/Pt]_{ML}$ has strong PMA; hence, moments of Fe at the interface will be aligned normal to the film plane due to dipolar coupling as observed through GINRS measurement for RT spectra. Thus, the absence of preferential pinning in the in-plane direction during the magnetization reversal of the IPA layer results in the absence of EB in the as-deposited sample. This also explains the absence of EB when the multilayer is annealed without a field. A strong in-plane field is required to rotate these moments in-plane to observe EB [12,16,17,21,22]. However, in the present study, magnetization reversal was studied as a function of H-annealing in a 1500 Oe magnetic field. The application of an in-plane magnetic field during annealing might create magnetic spins at the interface saturated along the direction of the applied magnetic field [52–55].

However, since the field is small compared to that required to reverse the $[Co/Pt]_{ML}$, a complete reversal of its moments in the in-plane direction will not occur [52]. This creates a net remanent in-plane magnetization, resulting in unidirectional anisotropy at the interface that pins the IPA layer and results in the appearance of EB (see Fig. 10). This is equivalent to the AFM/FM bilayer where an uncompensated moment at the interface pins the FM layer. GINRS study confirms the presence of magnetic spins at the interface with net in-plane remanent magnetization along the direction of the applied magnetic field. The rotation of moments in the direction of the applied field is in accordance with the literature, wherein

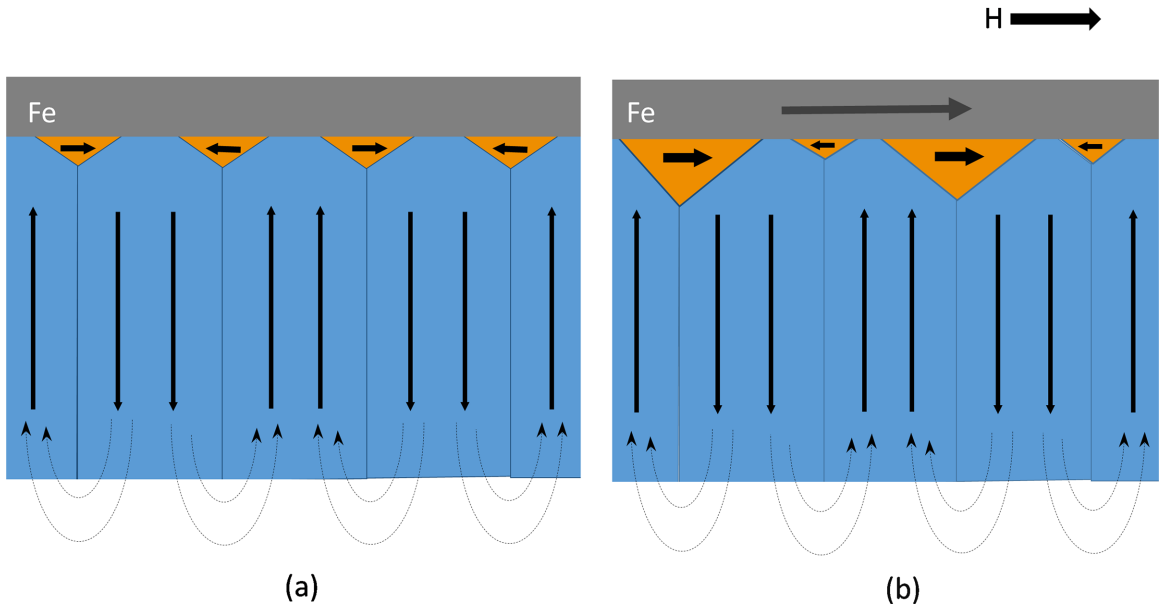

FIG. 10. Schematic representation of closure domains for the sample annealed (a) in the absence of a magnetic field and (b) in the presence of 1500 Oe magnetic field in the plane of the film.

annealing in the presence of a moderate magnetic field at a higher temperature assists the ordering of spin in the direction of the applied field [52–55]. Figure 10(a) shows that the remanent in-plane magnetization may result from asymmetrical closure domains at the interface parallel to the applied field [16–20]. This condition is otherwise absent when moments at the interface are perpendicular, or the closure domains are oriented uniformly [as shown in Fig. 10(b)].

In orthogonal magnetic anisotropy systems, the magnetic domains can be characterized by a mazelike domain pattern, where the magnetization is oriented perpendicular to the [Co/Pt] multilayer surface and also extends across Fe film, which is on top. At the domain walls between adjacent domains, closure domains form between adjacent domains of orthogonal magnetic anisotropic material to minimize the energy associated with the abrupt change in magnetization direction. The closure domains at the interface provide a pinned domain structure, which affects the reversal of the ferromagnetic layer and produces exchange bias. It also determines the magnitude and direction of the exchange bias effect and acts as nucleation sites for the formation of modified magnetic domains during the magnetization reversal process, which affects the overall coercivity of the system.

It may be noted that the strong PMA at the lower temperature leads to strong perpendicular coupling. Therefore, during annealing, the applied magnetic field may not be sufficient to pin interface spins in the film plane. Hence below 523 K, thermal energy coupled with a 1500 Oe magnetic field may be insufficient to orient the spins in-plane, resulting in the absence of EB. However, a further increase in the interface roughness and interdiffusion is responsible for significantly decreasing the PMA strength in $[Co/Pt]_{ML}$ [31]. It, in turn, increases interface pinning even in the magnetic field of 1500 Oe, applied during the field annealing. Thus, it results in an increase in the coupling between hard $[Co/Pt]_{ML}$ and soft Fe layer in the film plane, resulting in enhanced H_C and exchange bias above 523 K. This is per the similar work carried out in a Co/Pt multilayer system [18], where weakening of the PMA due to varying underlayer Pt buffer thickness increased exchange bias. Thus, in the present case, an observed unusual increase in H_C and the appearance of EB above 523 K in $[Co/Pt]_{ML}$/Fe multilayer with orthogonal anisotropy is attributed to the decreasing strength of PMA in $[Co/Pt]_{ML}$. The relatively weak PMA allows field annealing ($\sim$ 1500 Oe) to pin net spins in the film plane, resulting in unidirectional anisotropy through the closure domains at the interface.

IV. CONCLUSION

The magnetization reversal process of a soft ferromagnetic Fe layer coupled to a [Co/Pt] multilayer with perpendicular magnetic anisotropy (PMA) has been investigated. Through *in situ* investigations, we ensured that our results remained untainted by contamination, thereby enhancing the reliability and accuracy of our findings. We employ advanced techniques such as x-ray standing wave (XSW) and grazing incidence nuclear resonance scattering (GINRS) to achieve enhanced interface resolution. This rigorous methodology allowed us to obtain precise measurements, and it facilitated the study of magnetization reversal in the soft magnetic layer at the appropriate fields without disturbing the magnetic state of the hard magnetic layer. The magnetic orientation and magnitude at the interface of the two orthogonal magnetic anisotropic layers were examined by modifying the interface remanent state through annealing in a magnetic field. An emergence of exchange bias (EB) and an increase in coercivity (H_C) were observed when annealing was conducted in the presence of an in-plane magnetic field, whereas these effects were absent otherwise. This unusual behavior can be attributed to two

factors: (i) a decrease in interface roughness leading to an increase in PMA strength within the Co/Pt multilayer, and (ii) the net in-plane remanent magnetization induced at the interface by the applied magnetic field, resulting in unidirectional anisotropy and contributing to EB in the multilayer. The presence of closure domains at the interface is found to play a pivotal role in establishing a pinned domain structure, thereby influencing the reversal of the Fe layer and giving rise to the exchange bias effect. These closure domains dictate the magnitude and direction of the exchange bias and act as nucleation sites for the formation of altered magnetic domains during the magnetization reversal process. Consequently, the presence and characteristics of these closure domains significantly impact the overall coercivity of the system. The present work strives to shed light on the intricate nature of exchange bias in orthogonal magnetic systems, and to provide a clearer understanding of the interplay between exchange coupling, closure domains, and the origin of exchange bias.

ACKNOWLEDGMENTS

We acknowledge Deutsches Elektronen-Synchrotron (DESY) (Hamburg, Germany), a member of the Helmholtz Association HGF, for providing experimental facilities. We would also like to thank the Department of Science and Technology (DST), Government of India, for providing financial assistance (Project-CRG/2021/003094) and performing experiments at DESY, Hamburg, within the framework of the India@DESY collaboration (Proposal No. I-20160350). We acknowledge Er. Layant Behera and Prabhat Kumar, UGC-DAE CSR, Indore, India, for film deposition using the sputtering technique.

[1] W. H. Meiklejohn and C. P. Bean, Phys. Rev. **102**, 1413 (1956).
[2] J. Nogues and I. K. Schuller, J. Magn. Magn. Mater. **192**, 203 (1999).
[3] D. Kumar, S. Singh, and A. Gupta, J. Appl. Phys. **120**, 085307(2016).
[4] A. Berger, D. T. Margulies, and H. Do, Appl. Phys. Lett. **85**, 1571 (2004).
[5] A. Berger, D. Margulies, H. Do, A. Ktena, and K. Dahmen, J. Appl. Phys. **97**, 10K109 (2005).
[6] Z. Hussain, D. Kumar, V. R. Reddy, and A. Gupta, J. Magn. Magn. Mater. **430**, 78 (2017).
[7] S. Polisetty, S. Sahoo, A. Berger, and C. Binek, Phys. Rev. B **78**, 184426 (2008).
[8] S. Singh, D. Kumar, B. Bhagat, R. J. Choudhary, and V. R. Reddy, J. Phys. D **51**, 075006 (2018).
[9] J. Sort, V. Baltz, F. Garcia, B. Rodmacq, and B. Dieny, Phys. Rev. B **71**, 054411 (2005).
[10] S. Maat, K. Takano, S. S. P. Parkin, and E. E. Fullerton, Phys. Rev. Lett. **87**, 087202 (2001).
[11] S. M. Zhou, L. Sun, P. C. Searson, and C. L. Chien, Phys. Rev. B **69**, 024408 (2004).
[12] J. Jiang, T. Yu, R. Pan, Q.-T. Zhang, P. Liu, H. Naganuma, M. Oogane, Y. Ando, and X. Han, Appl. Phys. Express **9**, 063003 (2016).
[13] S. T. Lim, M. Tran, J. W. Chenchen, J. F. Ying, and G. Han, J. Appl. Phys. **117**, 17A731 (2015).
[14] A. Baruth and S. Adenwalla, J. Phys.: Condens. Matter **23**, 376002 (2011).
[15] A. Hierro-Rodriguez, J. M. Teixeira, M. Vélez, L. M. Alvarez-Prado, J. I. Martín, and J. M. Alameda, Appl. Phys. Lett. **105**, 102412 (2014).
[16] J. Sort, A. Popa, B. Rodmacq, and B. Dieny, Phys. Rev. B **70**, 174431 (2004).
[17] A. Bollero, L. D. Buda-Prejbeanu, V. Baltz, J. Sort, B. Rodmacq, and B. Dieny, Phys. Rev. B **73**, 144407 (2006).
[18] A. Bollero, V. Baltz, L. D. Buda-Prejbeanu, B. Rodmacq, and B. Dieny, Phys. Rev. B **84**, 094423 (2011).
[19] A. Bollero, L. D. Buda-Prejbeanu, V. Baltz, B. Rodmacq, and B. Dieny, IEEE Trans. Magn. **42**, 2990 (2006).
[20] S. Choi, S.-K. Bac, X. Liu, S. Lee, S. Dong, M. Dobrowolska, and J. K. Furdyna, Sci. Rep. **9**, 13061 (2019).
[21] D. Navas, J. Torrejon, F. Beron, C. Redondo, F. Batallan, B. P. Toperverg, A. Devishvili, B. Sierra, F. Castano, K. R. Pirota, and C. A. Ross, New J. Phys. **14**, 113001 (2012).
[22] N. Vukadinovic, J. Ben Youssef, V. Castel, and M. Labrune, Phys. Rev. B **79**, 184405 (2009).
[23] P. Y. Yang, X. Y. Zhu, F. Zeng, and F. Pan, Appl. Phys. Lett. **95**, 172512 (2009).
[24] A. Bollero, B. Dieny, J. Sort, K. S. Buchanan, S. Landis, and J. Nogues, Appl. Phys. Lett. **92**, 022508 (2008).
[25] A. G. Khanderao, I. Sergueev, H. C. Wille, and D. Kumar, Appl. Phys. Lett. **116**, 101603 (2020).
[26] L. Bocklage, C. Swoboda, K. Schlage, H.-C. Wille, L. Dzemiantsova, S. Bajt, G. Meier, and R. Röhlsberger, Phys. Rev. Lett. **114**, 147601 (2015).
[27] P. Chowdhury, P. D. Kulkarni, M. Krishnan, Harish C. Barshilia, A. Sagdeo, S. K. Rai, G. S. Lodha, and D. V. Sridhara Rao, J. Appl. Phys. **112**, 023912 (2012).
[28] A. Gupta, P. Rajput, A. Saraiya, V. R. Reddy, M. Gupta, S. Bernstorff, and H. Amenitsch, Phys. Rev. B **72**, 075436 (2005).
[29] A. Gupta, D. Kumar, C. Meneghini, and J. Zegenhagen, J. Appl. Phys. **101**, 09D117 (2007).
[30] M. S. Jamal, Y. Kumar, M. Gupta, P. Gupta, I. Sergeev, H. C. Wille, and D. Kumar, Hyperfine Interact. **242**, 17 (2021).
[31] See Supplemental Material at http://link.aps.org/supplemental/10.1103/PhysRevB.108.075414 for selecting the appropriate magnetic field for the hysteresis loop measurement and for decreasing strength of PMA with increasing temperature above 523 K, which includes Refs. [32,33].
[32] G. Sharma, U. P. Deshpande, D. Kumar, and A. Gupta, J. Appl. Phys. **112**, 023910 (2012).
[33] C.-Y. You and S.-C. Shin, J. Magn. Magn. Mater. **198**, 573 (1999).
[34] H.-C. Wille, H. Franz, R. Röhlsberger, W. A. Caliebe, and F.-U. Dill, J. Phys.: Conf. Ser. **217**, 012008 (2010).
[35] A. Gupta, D. Kumar, and V. Phatak, Phys. Rev. B **81**, 155402 (2010).

[36] A. Gupta, D. Kumar, and C. Meneghini, Phys. Rev. B **75**, 064424 (2007).
[37] L. G. Parratt, Phys. Rev. **95**, 359 (1954).
[38] M. T. Johnson, P. J. H. Bloemen, F. J. A. den Broeder, and J. j. de Vries, Rep. Prog. Phys. **59**, 1409 (1996).
[39] S. Bandiera, R. C. Sousa, B. Rodmacq, and B. Dieny, Appl. Phys. Lett. **100**, 142410 (2012).
[40] G. Sharma, R. Gupta, D. Kumar, and A. Gupta, J. Phys. D **46**, 505302 (2013).
[41] A. Tiwari, M. K. Tiwari, M. Gupta, H.-C. Wille, and A. Gupta, Phys. Rev. B **99**, 205413 (2019).
[42] S. Sumi, Y. Kusumoto, Y. Teragaki, K. Torazawa, S. Tsunashima, and S. Uchiyama, J. Appl. Phys. **73**, 6835 (1993).
[43] S. Gupta, R. Sbiaa, M. Al Bahri, A. Ghosh, S. N. Piramanayagam, M. Ranjbar, and J. Akerman, J. Phys. D **51**, 465002 (2018).
[44] Y. B. Zhang and J. A. Woollam, IEEE Trans. Magn. **31**, 3262 (1995).
[45] H. Kurt, M. Venkatesan, and J. M. D. Coey, J. Appl. Phys. **108**, 073916 (2010).
[46] R. Röhlsberger, K. Schlage, T. Klein, and O. Leupold, Phys. Rev. Lett. **95**, 097601 (2005).
[47] M. A. Andreeva, Hyperfine Interact. **185**, 17 (2008).
[48] http://www.esrf.eu/Instrumentation/software/data-analysis/OurSoftware/REFTIM-1.
[49] D. A. Gilbert, J.-W. Liao, B. J. Kirby, M. Winklhofer, C.-H. Lai, and K. Liu, Sci. Rep. **6**, 32842 (2016).
[50] B. Laenens, N. Planckaert, J. Demeter, M. Trekels, C. L'abbé, C. Strohm, R. Rüffer, K. Temst, A. Vantomme, and J. Meersschaut, Phys. Rev. B **82**, 104421 (2010).
[51] T. N. Anh Nguyen, Y. Fang, V. Fallahi, N. Benatmane, S. M. Mohseni, R. K. Dumas, and J. Åkerman, Appl. Phys. Lett. **98**, 172502 (2011).
[52] S. van Dijken, J. Moritz, and J. M. D. Coey, J. Appl. Phys. **97**, 063907 (2005).
[53] Y. B. Li, Y. F. Lou, L. R. Zhang, B. Ma, J. M. Bai, and F. L. Wei, J. Magn. Magn. Mater. **322**, 3789 (2010).
[54] L. Liu, H. Lv, W. Sheng, Y. Lou, J. Bai, J. Cao, B. Ma, and F. Wei, Appl. Surf. Sci. **258**, 5770 (2012).
[55] Z. Liu, W. Li, W. Fei, and D. Xu, J. Nanometer **2012**, 174735 (2012).